Chapter 1
Seismic Damage Assessment of a Full-Scale 10-Story Building Using UAV Vision-Based Sensing

Ruipu Ji, Hilda Lozano Bravo, Eric Lo, Tanner J. Norton, John W. Driscoll, Jiachen Zhang, Falko Kuester, and Tara C. Hutchinson

Abstract Seismic damage assessment is critical for safety evaluation and functional recovery of structures after earthquakes. Unmanned aerial vehicle (UAV) vision-based sensing has become an emerging technology supplementing and advancing conventional data collection practices for post-disaster evaluation due to its accessibility and efficiency. This study presents a UAV vision-based sensing application for damage assessment of a full-scale 10-story cold-formed steel (CFS) framed building during a series of shake table tests conducted at the 6 degree-of-freedom Large High-Performance Outdoor Shake Table (LHPOST6) at UC San Diego. The proposed damage assessment methodology integrates high-resolution aerial imagery collected before and after seismic tests and multiple image processing and computer vision algorithms to enable the assessment of structural and nonstructural damage with small scales. The location and scale of the damage is determined based on the thresholded absolute difference within the intensity normalized co-registered image pairs. A selected damage detection result using the proposed method applied on the north façade of the building is presented and compared to photogrammetry and manual inspection results. These findings highlight the potential of UAV vision-based sensing for post-earthquake reconnaissance, enabling assessment of even minor, small-scale damage realized during seismic excitations.

Keywords Unmanned Aerial Vehicle · Vision-Based Sensing · Image Processing · Shake Table Tests · Damage Assessment

Introduction

Unmanned aerial vehicle (UAV) vision-based sensing has emerged as a cost-effective approach supplementing and advancing conventional data collection practices for safety evaluation and functional recovery of infrastructure after earthquakes [1, 2]. Notable benefits of using UAV-based tools include its non-invasive and remote capture potential, aspects that are particularly useful for infrastructure with large scales. Besides tracking the structural displacement from the UAV-based imagery under seismic excitations [3–5], capturing the post-earthquake state of the structures for rapid and accurate assessment of structural and nonstructural damage is also critical. Researchers have been investigating the application of UAV vision-based sensing for seismic damage assessment for years with a focus on the major structural damage with a relatively large scale with respect to the size of the image frame [6, 7]. However, modern civil structures are more likely to have minor damage to the nonstructural components than to suffer extensive damage to the major structural members with the use of high-strength structural materials and improved structural design approaches [8]. Detection and assessment of such minor damage remain essential since they indicate early signs of structural deterioration and affect the overall safety and functionality of the structure.

This study investigates UAV vision-based sensing for damage assessment of a full-scale 10-story cold-formed steel (CFS) framed building during a series of shake table tests conducted at the 6 degree-of-freedom Large High-Performance

Ruipu Ji · Jiachen Zhang · Falko Kuester · Tara C. Hutchinson
Department of Structural Engineering, University of California San Diego
e-mail: r5ji@ucsd.edu; jiz149@ucsd.edu; fkuester@ucsd.edu; tara@ucsd.edu

Hilda Lozano Bravo · Eric Lo · Tanner J. Norton · John W. Driscoll
Qualcomm Institute, University of California San Diego
e-mail: hlozanobravo@ucsd.edu; eklo@ucsd.edu; tanorton@ucsd.edu; jwdrisco@ucsd.edu

© The Author(s), under exclusive license to River Publishers 2026

Kristin B. Zimmerman, PhD (eds.), *Dynamics of Civil Structures, 2026, Vol. 2*, Conference Proceedings of the Society for Experimental Mechanics Series, https://doi.org/10.13052/rp-9788743814139

Outdoor Shake Table (LHPOST6) at UC San Diego. The schedule and implementation plan for two UAV vision-based inspection approaches during the seismic test program are presented including photogrammetry and image-based inspection. A damage assessment methodology for the image-based inspection is proposed, which integrates high-resolution aerial imagery collected before and after the seismic test and multiple image processing and computer vision algorithms to enable the assessment of structural and nonstructural damage observable at small scales. The location and scale of the damage is extracted by the thresholded absolute difference within the intensity normalized co-registered image pairs with baseline (pre-test) and damage (post-test) images. The proposed methodology is illustrated using a selected damage from the exterior insulation finishing system (EIFS) on the north façade of the building. The damage detected by the image-processing based methodology shows reasonable agreement with photogrammetry results and manual inspection results.

UAV Vision-Based Seismic Damage Assessment Plan for CFS10 Seismic Test Program

A full-scale 10-story cold-formed steel (CFS) framed building, coined CFS10, was constructed and tested under a series of shake table tests [9] at the 6-DOF Large High-Performance Outdoor Shake Table (LHPOST6) [10] at UC San Diego. The CFS10 building has a total height of 30.5 m (to the roof level) and a floor plan measuring 6.86 m × 11.58 m as shown in Fig. 1(a). In addition to the load bearing CFS studs and CFS-sheathed shear walls, the building was detailed with various nonstructural components including an exterior face with a stucco-based exterior insulation and finishing system (EIFS) on the north side of the building. Stucco-based EIFS is a common exterior finish system for CFS buildings, though it has lower strength compared to CFS structural components and nonstructural drywall systems. Therefore, it is more likely to be damaged during extreme events such as earthquakes. A pair of images of a cracked region from the EIFS on the north side of the building is selected as an example to illustrate the proposed damage detection methodology.

A series of shake table tests with 18 multi-directional earthquake motions scaled to various hazard levels were performed on the CFS10 building as presented in Table 1 [9, 11]. The UAV vision-based seismic damage assessment flights were conducted following significant milestones during the test program, applying two different sensing approaches, namely photogrammetry inspection and image-based inspection as shown in Fig. 1(b) and 1(c). For the photogrammetry inspection, which aimed at creating a digital twin for the building specimen, a quadrotor UAV with real-time kinematic (RTK) support (DJI Matrice 300 RTK) equipped with a 45-megapixel resolution image sensor (DJI Zenmuse P1 camera) and 24 mm lens, was deployed in a vertical lawnmower flight pattern for each side of the building followed by a horizontal lawnmower pattern for the roof [12, 13]. Details of the photogrammetry model development are provided in Lozano Bravo et al. [13]. The image-based inspection, which aimed for direct comparison between images captured after each test phase, utilized a small quadrotor UAV (DJI Mini4 Pro) with its default onboard camera, and the flight was conducted in the vertical lawnmower pattern around the building. The UAV hovered in front of each structural or nonstructural component of interest at a distance varying between 1 and 5 m from the building façade to cover the entire exterior of the building including exterior drywalls, windows, exterior door openings, and exterior insulation finishing system (EIFS). Table 2 presents the specifications of the UAV platforms and the camera models used for inspection flights, while Table 3 presents the raw image collection from

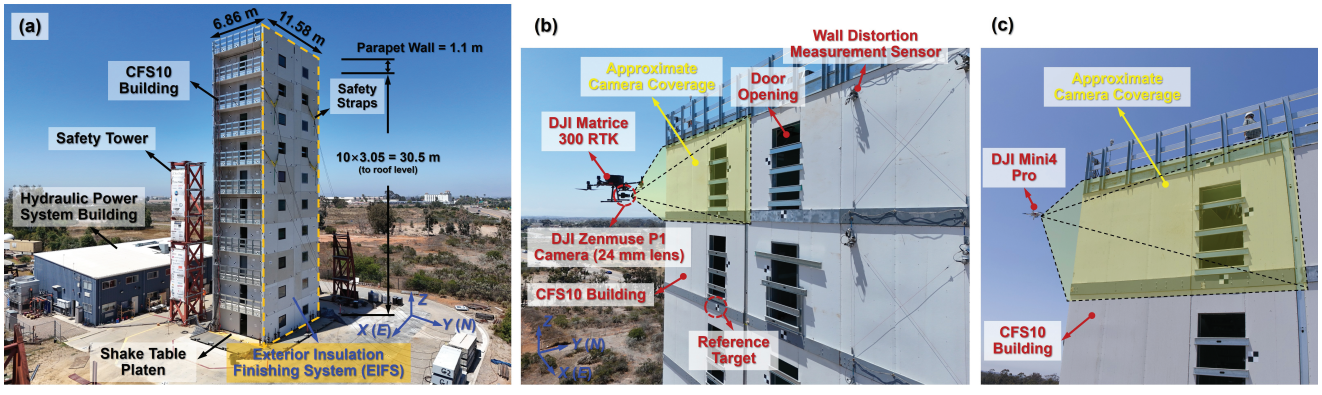

Fig. 1 Overview of the CFS10 building specimen and image collection for the UAV vision-based post-earthquake structural damage assessment: (a) Northeast aerial view of the CFS10 building, (b) Photogrammetry inspection flight, (3) Image-based inspection flight.

Table 1 Seismic test protocol imposed on the CFS10 building and schedule for UAV vision-based structural inspection [9, 11].

Hazard Level	MID[1]	Earthquake Event				Input DOF	Components		$D_{5\text{-}95}$[2] [sec]	Achieved Peak Input Acceleration [g]		
		Name, Location	Year	M_w	Recording Station		X	Y		X	Y	Z
Photogrammetry Inspection #1												
Image-Based Inspection #1												
SLE[3]	1[4]	Loma Prieta, California	1989	6.9	Gilroy Array #3	XYZ	90°	0°	11.4	0.126	0.122	0.082
Image-Based Inspection #2												
SLE	2	Loma Prieta, California	1989	6.9	Gilroy Array #3	XYZ	90°	0°	11.4	0.118	0.114	0.096
	3					X	90°		11.4	0.133	0.041	0.025
	4					Y		0°	6.4	0.042	0.109	0.024
	5	Northridge, California	1994	6.7	LA City Terrace	XYZ	90°	180°	11.9	0.125	0.121	0.081
	6					XYZ	180°	90°	11.9	0.184	0.094	0.084
	7					X	180°		11.9	0.168	0.027	0.023
	8					Y		90°	11.6	0.026	0.093	0.021
	9	Cape Mendocino, California	1992	7.0	Rio Dell Overpass	XYZ	270°	360°	15.3	0.084	0.109	0.099
	10					XYZ	360°	270°	15.3	0.078	0.122	0.151
	11[5]	Kahramanmaras, Türkiye	2023	7.8	4611	XYZ	E	N	43.4	0.095	0.075	0.050
	12					XYZ	E	N	43.4	0.117	0.110	0.064
	13	Elbistan, Türkiye	2023	7.5	4611	XYZ	E	N	35.1	0.100	0.061	0.052
	14	Maule, Chile	2010	8.8	Curico Hospital	XY	EW	NS	45.2	0.097	0.091	0.033
Photogrammetry Inspection #2												
Image-Based Inspection #3												
SLE	15	Kahramanmaras, Türkiye	2023	7.8	4611	XYZ	E	N	43.4	0.119	0.089	0.063
DE[3]	16	Loma Prieta, California	1989	6.9	Gilroy Array #3	XY	90°	0°	11.4	0.454	0.388	0.014
Photogrammetry Inspection #3												
Image-Based Inspection #4												
MCE_R[3]	17	Loma Prieta, California	1989	6.9	Gilroy Array #3	XY	90°	0°	11.4	0.723	0.619	0.016
Photogrammetry Inspection #4												
Image-Based Inspection #5												
MCE_R	18	Cape Mendocino, California	1992	7.0	Rio Dell Overpass	XY	360°	270°	15.3	0.782	0.336	0.025
Photogrammetry Inspection #5												
Image-Based Inspection #6												

[1] MID = motion identification.
[2] $D_{5\text{-}95}$: Significant duration of strong shaking computed as the time interval between 5% and 95% Arias Intensity per original record (max component).
[3] SLE = service level earthquake, DE = design earthquake, and MCE_R = risk-targeted maximum considered earthquake.
[4] MID1 was conducted with the stairs in a locked configuration.
[5] MID11 was targeted to 75% SLE.

Table 2 Specifications of the UAV platforms and camera models for CFS10 post-earthquake structural inspection [14].

UAV Model	Inspection Type	Unfolded Size [$L \times W \times H$-mm]	Battery Life [min]	Camera Model	Image Resolution
DJI Matrice 300 RTK	Photogrammetry	810×670×430	55	DJI Zenmuse P1 camera (24 mm lens)	8192×5460
DJI Mini4 Pro	Image-based	298×373×101	39	Default onboard camera	8064×6048

Table 3 Statistics of the raw image collection for CFS10 post-earthquake structural inspection.

Inspection Event	Image-Based Inspection		Photogrammetry Inspection	
	Inspection #	Raw Image Count	Inspection #	Raw Image Count
Pre-test	#1	199	#1	1920
End of locked stairs configuration	#2	177	-	-
End of SLE test phase	#3	156	#2	1931
End of DE test phase	#4	276	#3	2442
End of the 1st MCER test	#5	235	#4	2809
End of the 2nd MCER test	#6	246	#5	2493

photogrammetry inspection flights and image-based inspection flights statistics, as obtained during the CFS10 seismic test program.

Damage Detection Based on Intensity Normalized Co-Registered Image Pairs

This section presents the seismic damage detection methodology proposed for use with the imagery collected from the image-based inspection flights, see Fig. 2. The general idea is to extract the thresholded absolute difference between the intensity normalized co-registered image pairs with baseline (pre-test) and damage (post-test) images. For the scope of this paper, a selected crack damage at the upper-right corner of the Level 8 west window from the EIFS on the north façade of the building is presented for illustration purposes. The baseline image without damage was captured during image-based inspection #1 before MID1 and the damage image was captured during image-based inspection #6 at the end of the seismic test program.

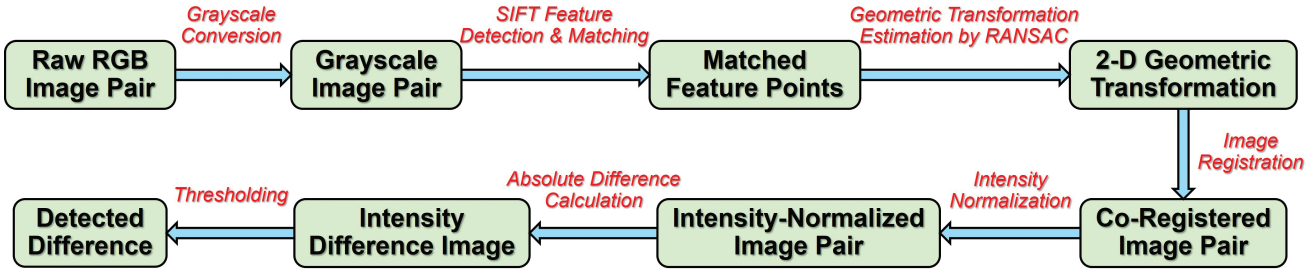

Fig. 2 Flowchart of the proposed damage detection methodology.

The following procedures are applied in the proposed method: (1) The raw RGB images are converted into grayscale for reduced computational cost as shown in Fig. 3. (2) Scale-invariant feature transform (SIFT) is applied to both grayscale images for feature detection and matching. (3) Given the matched SIFT feature points, the random sample consensus (RANSAC) algorithm is applied to remove the outliers and make a robust estimation for the 2-D geometric transformation from the baseline image to the damage image as presented in Fig. 4. (4) A pair of co-registered images (Fig. 5) is obtained by applying the 2-D geometric transformation to the damage image. (5) The damage image is normalized by multiplying a scale factor to ensure the non-zero part in the co-registered damage image has the same average intensity as the baseline image, where the intensity difference caused by the various lighting conditions is largely reduced. (6) The final detected difference is calculated as the thresholded absolute difference between the baseline image and intensity-normalized co-registered damage image as the binary image in Fig. 6(a), where the white pixels are considered as difference between baseline image and damage image.

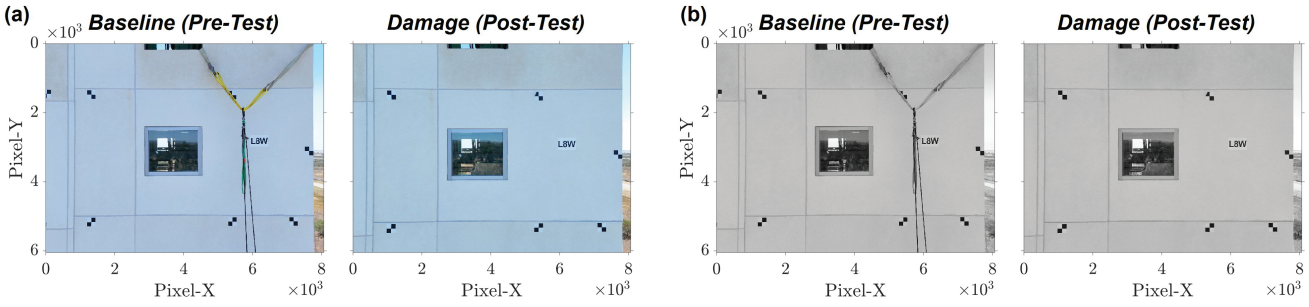

Fig. 3 (a) Raw RGB images captured by UAV, and (b) Converted grayscale images.

It is noted that the binary image result represents all detected differences between the baseline (pre-test) and damage (post-test) image. Therefore, it may include other non-damage differences in the test scene. For the presented example, the non-damage differences include the removal of the safety straps around the building and the difference caused by the various reflection from the window glazing. The final candidate damage could be extracted by excluding the known non-damage differences in the detection result. In addition, the scale of the damage could be estimated from the pixel resolution of the

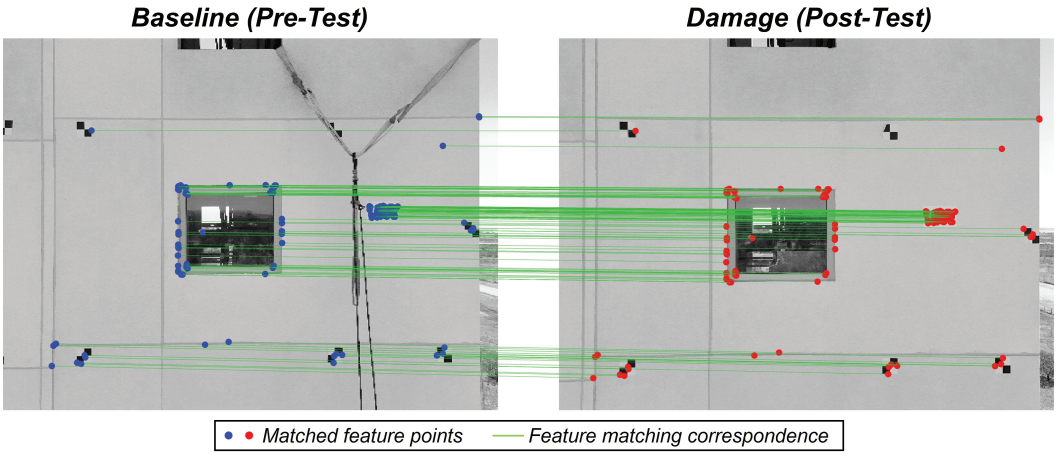

Fig. 4 Inliers of matched features from geometric transformation estimation by RANSAC algorithm.

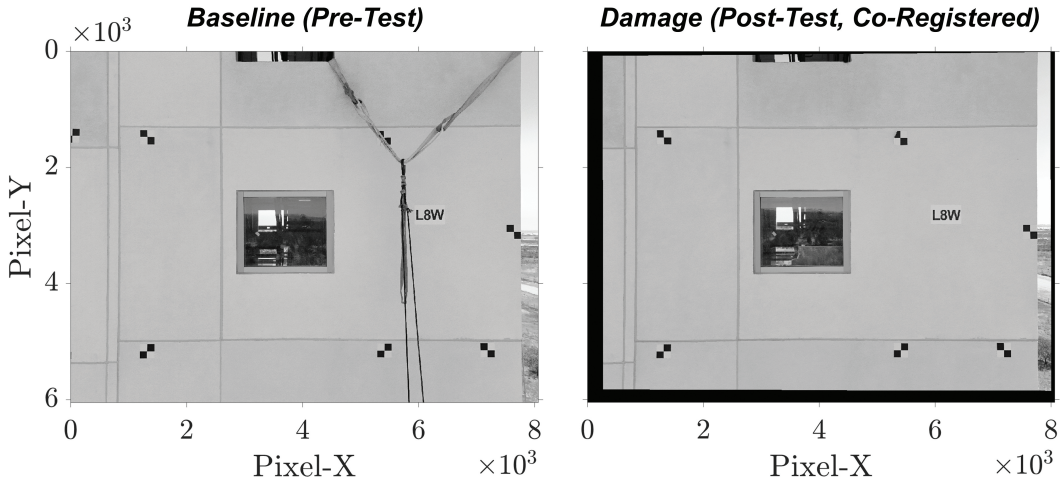

Fig. 5 Co-registered grayscale image pair after geometric transformation.

image extracted from features with known dimensions in the image frame. In the presented case, the pixel resolution of the image frame is 0.85 mm/pixel extracted using the black-and-white checkerboard reference target on the building façade as shown in Fig. 6(b). The total scale of the detected damage is extracted as 104 pixels which correspond to 8.84 cm in length.

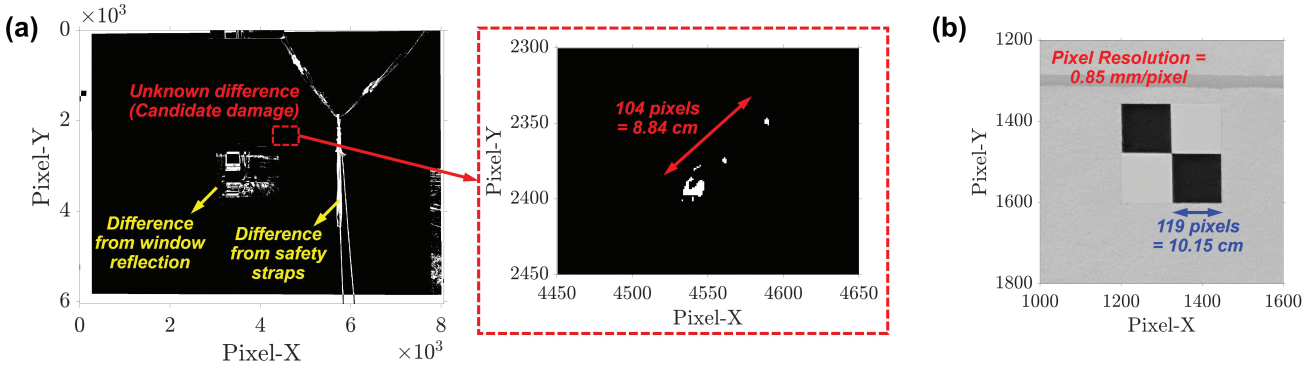

Fig. 6 (a) Detected difference with zoom-in view for candidate damage, and (b) Pixel resolution calculation using features with known dimensions from the pre-test grayscale image.

Discussion and Conclusions

For the selected crack damage located at the upper-right corner of the Level 8 west window from the EIFS on the north façade of the building, the damage is successfully located and extracted with an identified length of 8.84 cm. Fig. 7 presents the same damage observed from a point cloud model based on photogrammetry and a close-up view obtained with manual inspection using a traditional digital single-lens reflex (DSLR) camera. The length of the crack was measured as around 15 cm from the point cloud model and around 8.75 inches (22.23 cm) from the manual inspection. Although it is noted that the scale of the damage extracted from the image-based inspection and photogrammetry inspection are smaller than the actual dimension measured during manual inspection as shown in Fig. 7(b), the proposed damage detection methodology for image-based inspection could provide rapid localization and coarse scale estimation using the UAV-captured images with minimized manual operations.

The presented results offer preliminary results for a comprehensive damage assessment of the CFS10 building, and aid in evaluating the feasibility of a proposed UAV vision-based damage assessment methodology. The method involves extraction of the location and scale of the damage by calculating the thresholded absolute difference within the intensity normalized co-registered image pair with baseline (pre-test) and damage (post-test) images. These findings highlight the potential of UAV vision-based sensing for post-earthquake reconnaissance, enabling assessment of even minor or small-scale damage under seismic excitations.

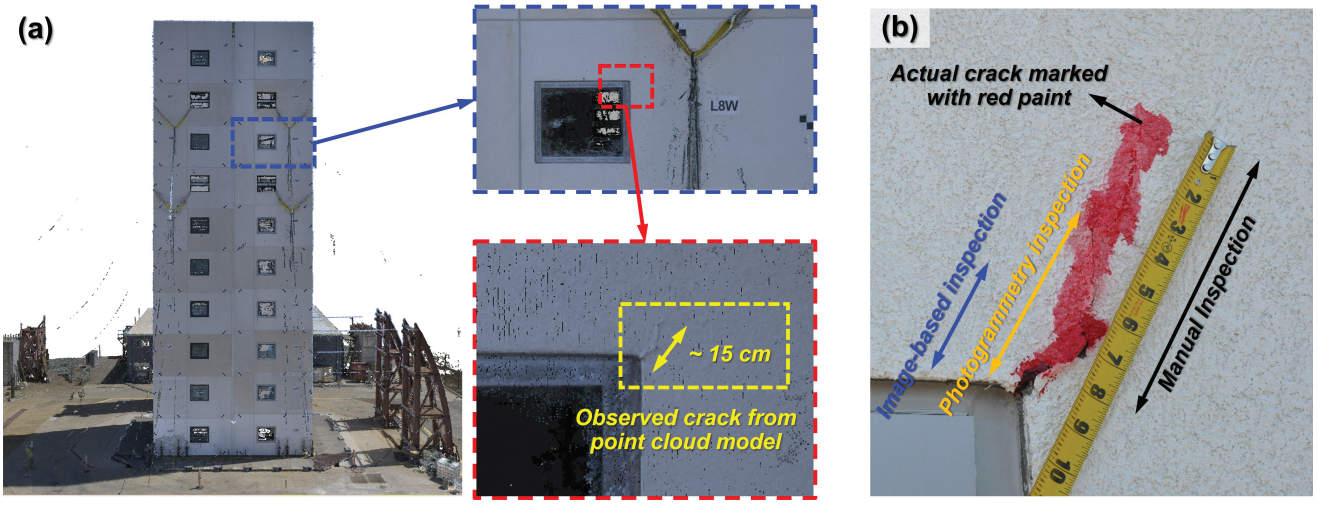

Fig. 7 Crack at the upper-right corner of the L8 west window observed from (a) point cloud model based on photogrammetry, and (b) close-view manual inspection.

Acknowledgments This research is funded by the California Office of Emergency Services (CalOES) and the California Seismic Safety Commission (CSSC) with Agreement #A211006635. The CFS-NHERI 10-story building capstone test program is supported by the National Science Foundation (NSF) with CMMI 1663569 and 1663348 (project entitled: Collaborative Research: Seismic Resiliency of Repetitively Framed Mid-Rise Cold-Formed Steel Buildings), and numerous federal/state and industry partners (listed at: cfs10.ucsd.edu/sponsors-partners). The efforts of all undergraduate and graduate students, visiting scholars (listed at: cfs10.ucsd.edu/people), and the technical support from the LHPOST6 staff (listed at: nheri.ucsd.edu/about/personnel) are greatly appreciated. Findings, opinions, and conclusions are those of the authors and do not necessarily reflect those of the sponsoring organizations.

References

1. Terzic, V., Villanueva, P.K., Saldana, D., and Yoo, D.Y. (2021). Framework for modelling post-earthquake functional recovery of buildings. *Engineering Structures*, 246: 113074. DOI: https://doi.org/10.1016/j.engstruct.2021.113074.
2. Hariri-Ardebili, M.A., and Speicher, M.S. (2025). Reconnaissance-informed post-earthquake functional recovery: Observations and challenges. *Earthquake Spectra*, 41 (1): 88-125. DOI: https://doi.org/10.1177/87552930241290488.
3. Ji, R., Sorosh, S., Lo, E., Norton, T.J., Driscoll, J.W., Kuester, F., Barbosa, A.R., Simpson, B.G., and Hutchinson, T.C. (2025). Application framework and optimal features for UAV-based earthquake-induced structural displacement monitoring. *Algorithms*, 18 (2): 66. DOI: https://doi.org/10.3390/a18020066.

4. Cao, P., Ji, R., Ma, Z., Sorosh, S., Lo, E., Norton, T., Driscoll, J., Wang, X., Hutchinson, T., Pei, S., and Kuester, F. (2024). UAV-based video analysis and semantic segmentation for SHM of earthquake-excited structures. *Proceedings of the 18th World Conference of Earthquake Engineering*, Milan, Italy. 2024.
5. Ji, R., Zhang, J., Lo, E., Norton, T.J., Driscoll, J.W., Kuester, F., Schafer, B.W., Hutchinson T.C. (2026). Multi-view UAV-based imagery for seismic displacement tracking of a full-scale 10-story cold-formed steel building. *Proceedings of the 13th National Conference on Earthquake Engineering*, Portland, OR.
6. Liu, Z., Xue, J., Wang, N., Bai, W., and Mo, Y. (2023). Intelligent damage assessment for post-earthquake buildings using computer vision and augmented reality. *Sustainability*, 15: 5591. DOI: https://doi.org/10.3390/su15065591.
7. Cheng, M.-Y., Sholeh, M.N., and Kwek, A. (2024). Computer vision-based post-earthquake inspections for building safety assessment. *Journal of Building Engineering*, 94: 109909. DOI: https://doi.org/10.1016/j.jobe.2024.109909.
8. Bianchi, S., Ciurlanti, J., and Pampanin, S. (2021). Comparison of traditional vs low-damage structural and non-structural building systems through a cost/performance-based evaluation. *Earthquake Spectra*, 37 (1): 366-385. DOI: https://doi.org/10.1177/8755293020952445.
9. Hutchinson, T.C., Eladly, M., Ji, R., Rivera, D., Rukundo, F.C., Singh, A., Sorosh, S., Zhang, J., Zhang, X., Padgett, L., Jones, H., Karns, J., and Schafer B.W. (2026). Advancing use of cold-formed steel framing systems for mid-rise residential construction in seismic zones via full-scale shake table testing. *Proceedings of the 8th Residential Building Design & Construction Conference*, State College, PA.
10. McCartney, J.S., Van Den Einde, L., Morrison, M., Palermo, A., Lotfizadeh, K., Lai, C.-T., and Conte, J.P. (2025). Multi-degree of freedom shake table testing of large-scale structural and geotechnical systems with NHERI-UCSD LHPOST6. *Frontiers in Built Environment*, 11: 1573390. DOI: https://doi.org/10.3389/fbuil.2025.1573390.
11. Zhang, J., Sorosh, S., Ji, R., Lotfizadeh, K.H., Schafer, B.W., Hutchinson, T.C. (2026). Full-scale 10-story cold-formed steel building shake table test: Protocol development and shake table performance. *Proceedings of the 13th National Conference on Earthquake Engineering*, Portland, OR.
12. Driscoll, J., Lo, E., Norton, T., Ji, R., Hutchinson, T., Driscoll, N., Kuester, F. (2026). Unmanned aerial vehicle (UAV) flight strategies for post-earthquake inspections. *Proceedings of the 13th National Conference on Earthquake Engineering*, Portland, OR.
13. Lozano Bravo, H., Ji, R., Lo, E., Norton, T., Driscoll, J., Zhang, J., Zazueta Hernandez, I., Romo Andrade, A., Hutchinson, T.C., Kuester, F. (2026). Post-earthquake damage assessment using a UAV-acquired photogrammetry model. *Proceedings of the 13th National Conference on Earthquake Engineering*, Portland, OR.
14. DJI - Official Website. Available from: https://www.dji.com/ (accessed on 27 September 2025).